ELSEVIER

Restrained Crack Widening in Mode I Crack Propagation for Mortar and Concrete

A. Turatsinze and A. Bascoul
Laboratoire Matériaux et Durabilité des Constructions, INSA-UPS Complexe Scientifique de Rangueil, Toulouse Cedex France

Microscopical observations and macroscopical investigations of the crack propagation process have been carried out. They give a new insight into the fracture process zone, leading one to presume that during the crack propagation the crack opening is restrained. So, the crack opening cannot increase without an energy dissipation that has to be added to the one from the crack propagation. Generally, measurements of fracture energy per unit of crack surface give rise to size dependent values for mortar and concrete. We propose a simple model that takes into account the energy dissipated by restrained crack widening (RCW), with the aim to verify if it can explain the size dependence on the energy dissipated per unit of crack surface. The theoretical predictions from the proposed model and the experimental dissipated energy per unit of crack surface obtained by means of RILEM TC-50 procedure are in good agreement. So, size dependence could be mainly explained through the concept of RCW. ADVANCED CEMENT BASED MATERIALS 1996, 4, 77–92

KEY WORDS: Crack roughness, Critical crack opening, Fracture energy, Mortar, Restrained crack widening (RCW), Size dependence

The knowledge of mortar and concrete fracture mechanisms is generally based on indirect methods of investigation of the material damage like the acoustic emission technique, the interferometry technique, or the X-ray method [1].

Some results obtained by direct observation are available. The technique of impregnation is one of the techniques that points out the crack surface at the macroscopic scale. It has been used to measure the specific fracture energy according to the crack propagation [2,3]. It has also been successfully used by Van Mier [4] who shows that the crack surfaces are interconnected by aggregate bridging, which gives a residual carrying capacity to the damaged material.

The replica technique in conjunction with scanning electron microscopy also allows direct observation of the fracture mechanism of mortar and concrete at the microscopic scale [5]. Wet specimens can be observed. Consequently, there are no microcracks induced by desiccation that could be wrongly considered as resulting from mechanical damaging. We have used this method to observe the fracture process of notched mortar specimens in mode I crack opening (three-point bending tests on notched beams) [6–9]. The main results discussed are relative to the composition and the specimen geometry specified in Table 1 and Figure 1.

The observations have been carried out on the lateral surface of the specimens and inside the specimens after cutting. Some 56 tests have been performed, and the following is the summary of our observations.

On the lateral surfaces, results show that, at the resolution of the method (0.1 μm), the crack initiation always appears before the peak load as a single microcrack (photograph in Figure 2), which propagates with some branchings but without formation of a cloud of microcracks neither ahead of nor around the main crack (Figure 3a).

Inside the material, at a given load beyond the peak load, the main crack path is continuous but always followed by discontinuous microcracks (Figure 3b).

The compilation of these results and the comparison with the ones from the impregnation technique lead to the model of fracture shown in Figure 4, a plane representation of a phenomenon that develops over a nonplane surface. A similar physical model was also proposed by Rossi [10].

The discontinuous microcracks observed inside the specimen are not distributed at random. They are located on a sinuous path (see Figure 3b) that marks the

Address correspondence to: Professor A. Bascoul, Laboratoire Materiaux et Durabilite des Constructions, INSA-UPS, Genie Civil Complexe Scientifique de Rangueil, 31077 Toulouse Cedex, France.
Received September 4, 1995; Accepted February 19, 1996

ISSN 1065-7355/96/$15.00
PII S1065-7355(96)00039-9

Advn Cem Bas Mat
1996;4:77–92

TABLE 1. Mix proportions and properties

Components	Amount
Water (l/m^3)	296
Cement CPA HP (kg/m^3)	557
Aggregate (kg/m^3)	1455
Maximum aggregate size (mm)	3.15
Compressive strength σ_c (MPa)	47.5
Young modulus (GPa)	27.1

future path of the continuous crack. The length of the microcracked zone can be regarded as the length of the well-known fracture process zone. This derives from comparisons we have made [7] with the two parameter model and the effective crack model [11]. As the crack opening is increased, the ligaments between the unconnected microcracks are broken. In this way, the continuous crack front progresses until the specimen fails.

The energy necessary for the initiation and the propagation of the microcracks in the process zone must not be seen in isolation because it is a part of the energy necessary for the formation of the future continuous crack. However, several phenomena act in opposition to the crack widening. These phenomena involve an energy dissipation when the crack opening is increased. In this paper, the term restrained crack widening (RCW) is used to designate all the mechanisms that hinder the increase of the crack opening, namely, interlocking, friction due to the sinuous crack path, crack deflection, and aggregate bridging.

These effects lead us to consider that the stresses across the crack are not strictly zero for concrete, as Shah has reminded us [12]. We have also confirmed the existence of the RCW by a very simple test. After a mechanical test, a specimen was sawn in two pieces A and B (Figure 5). Next, microscopical observations revealed a continuous crack path along the totality of the ligament of piece A. However, some force was required to make possible an effective separation of the two parts of piece A in spite of the continuous crack path. This required force is the result of the RCW. Moreover, as RCW hinders the increase of the crack opening, it may also prevent the crack from closing completely when a partially cracked specimen is unloaded. The replica technique made it possible to observe the tip of the crack of the same specimen loaded and unloaded. On the lateral surface, it has been recorded that the same crack length is observed in both cases [9]. Thus, we can deduce that the specimen remains self-stressed, and the crack cannot completely close in spite of the specimen unloading.

Size dependence is observed in the overall fracture energy G_F measured by the RILEM TC-50 procedure [13]. As an example, Figure 6 gives results reported by Karihaloo and Nallathambi [11] in a contribution by Elices and Planas. These results are interpreted as leading to an asymptotic variation of G_F according to the depth of the specimens. Indeed the overall fracture energy measured by the RILEM TC-50 procedure includes the energy necessary for the propagation of the crack along the specimen ligament and the energy dissipated by RCW. No doubt there are other sources of energy dissipation. As a matter of fact, acoustic emissions revealed some events beside the main path of the crack (see, for example, the observations of Rossi [10] in double cantilever beam (DCB) tests). On the other hand, strain field measurements pointed out tensile deformations greater than the tensile strain corresponding to the maximum stress reached under direct tension tests [14]. Such considerations can be regarded as consistent with the crack band model of Bazant [15].

However, considering the resolution of our observations, we think that the major amount of energy dissipation takes place along the path of the crack, first, for propagation and RCW during the crack growth stage, and, next, solely by RCW when all the microcracks are connected. Hence, the RCW physical concept could mainly explain the observed size dependence. Therefore, the remainder of this article deals with a model established from this concept in order to explain the variation of the fracture energy per unit of crack surface with both the length of the initial ligament and the crack opening level.

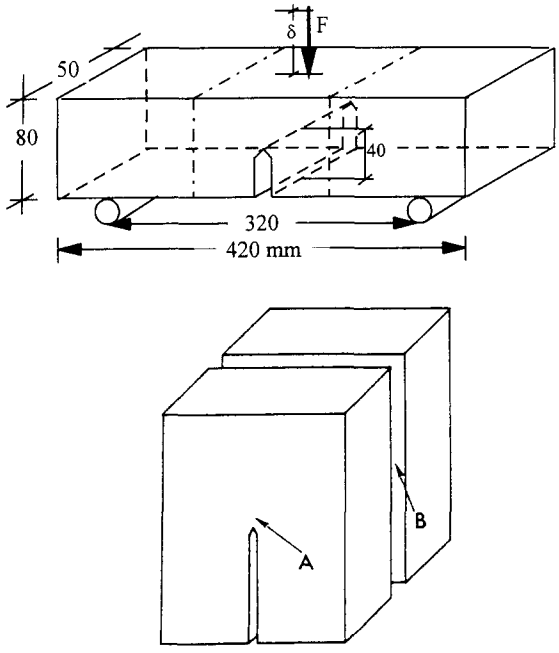

FIGURE 1. Test specimen and planes of observation; lateral surface (A) and median longitudinal plant (B).

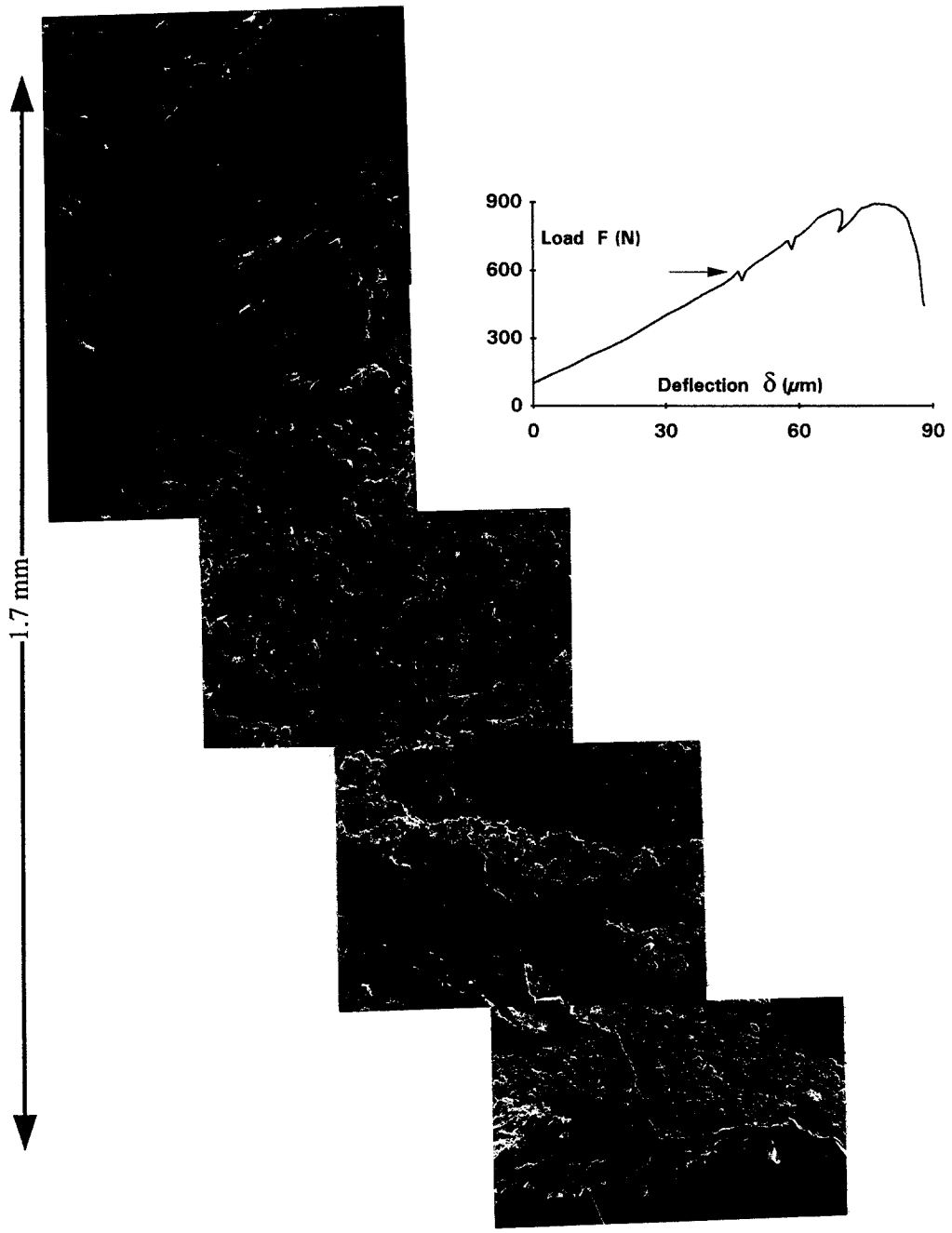

FIGURE 2. Crack initiation on the lateral surface; photograph of the zone at the notch tip.

Restrained Crack Widening and Fracture Energy Modeling

In mortar and concrete, several mechanisms contribute to the tendency of the main crack to follow a sinuous path. The model proposed in this paper is based on the idea that RCW results essentially from the roughness of the crack surface. This roughness may be characterized by the linear roughness R_l defined as the ratio between the developed crack length and its projection on the main crack direction. This is illustrated in Figure 7.

Next, we will consider that the measured fracture energy is an apparent fracture energy E_A, which can be regarded as a sum of two terms E_C and E_Φ.

$$E_A = E_C + E_\Phi \tag{1}$$

where E_C is the energy necessary for the initiation and the propagation of the crack, whereas E_Φ is the energy dissipated by RCW during the increase of the crack opening.

If the projected crack surface is S, we can deduce the fracture energy per unit of crack surface γ_A:

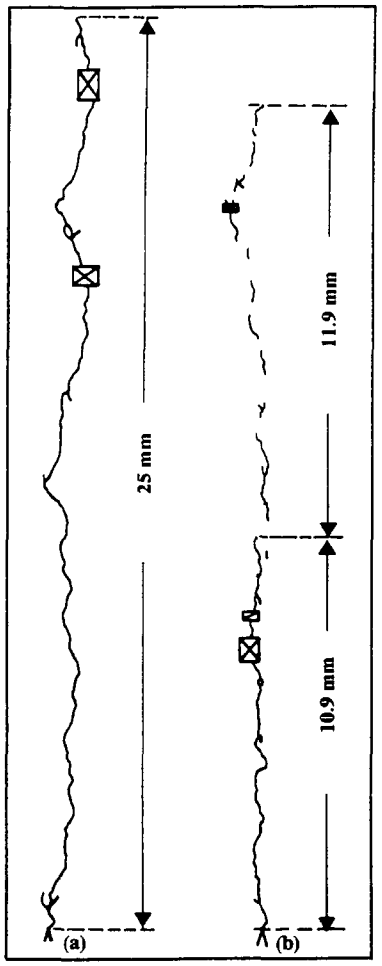

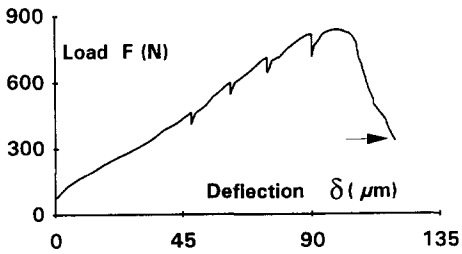

FIGURE 3. Map of the crack path. Lateral surface (a) and medium longitudinal plane (b). The arrow indicates the corresponding load-displacement level.

$$\gamma_A = \frac{E_C}{S} + \frac{E_\Phi}{S} = \gamma_C + \gamma_\Phi \qquad (2)$$

The term γ_C can be regarded as a characteristic parameter identified with the specific fracture energy in Griffith's sense to which is added the varying term γ_Φ, associated with RCW. So, we have to show that size dependence can be justified by the term γ_Φ.

Here, one can remark that following the calculation of the energy per unit of crack surface using the crack surface projection, some caution needs to be used in the interpretation of the results because of the roughness of the crack. In fact, fracture of materials of different compositions may be characterized by different linear roughnesses and, for instance, one can associate different developed crack surfaces with identical projected crack areas. In such conditions, comparisons of values of the energy per unit of crack surface from different compositions become relative in character, because these energies depend on the definition of the crack surface under consideration.

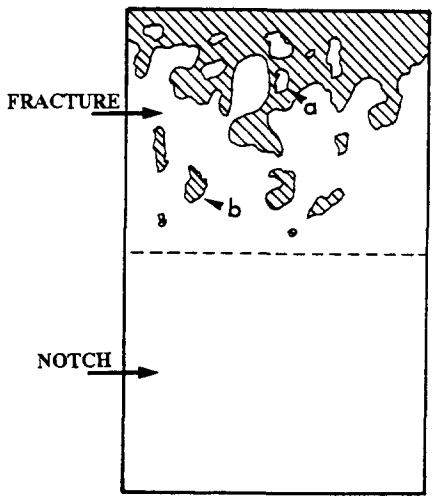

FIGURE 4. Model of fracture according to microscopical and macroscopical observations; microcrack (a) and material bridging (b).

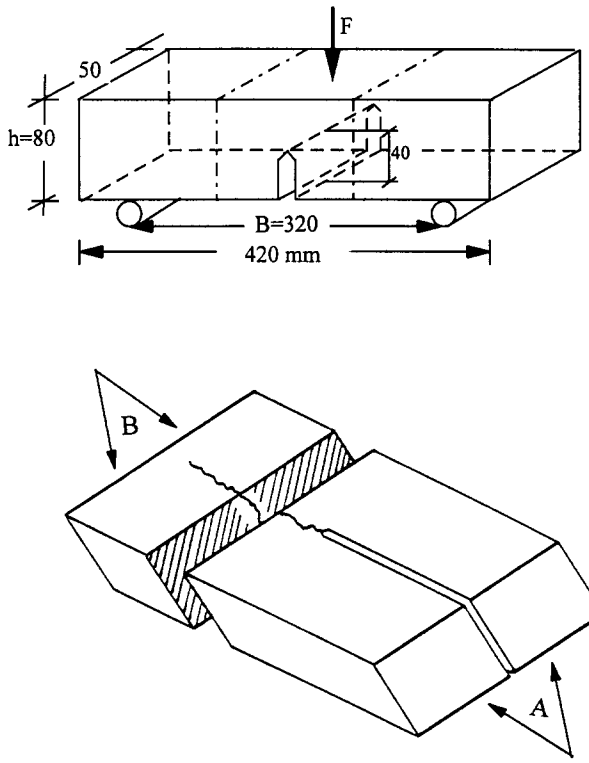

FIGURE 5. Effect of restrained crack widening. There is no effective separation of the two parts of the piece A in spite of continuous crack path.

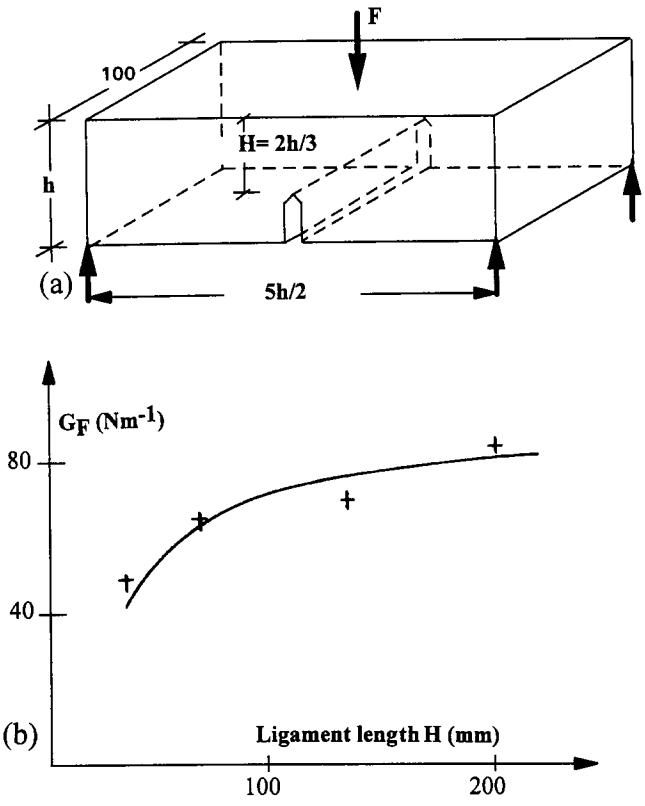

FIGURE 6. (a) Specimen geometry (H = 200, 133.3, 66.7, and 33.6 mm); (b) fracture energy (G_F) according to the initial ligament length (H) (from Kalihaloo and Nallathambi [11]).

Descriptive Hypotheses

Let us consider a sample whose width is equal to the unit. As a crack profile, we consider a periodic crack path characterized by the step length α (see Figure 8) and by the linear roughness R_l. Any i step of the crack profile can be located by Y_i with:

$$Y_i = i\alpha - \frac{\alpha}{2} \tag{3}$$

The specimen ligament length H is greater than the length of one step:

$$H = n\alpha, \quad \text{with } n \gg 1 \tag{4}$$

We consider that at every step, a resultant force Φ perpendicular to the direction of the mean crack plane acts in opposition to the increase of the crack widening, as long as the mean crack opening Δ_i does not exceed a critical value Δ_c, which is characteristic of an effective separation of the two crack surfaces. This force may be written like:

$$\Phi = K(R_l - 1) \tag{5}$$

where K is a coefficient that has a force dimension. It allows us to characterize crack profiles with different shapes but with the same linear roughness. So we can ascertain that Φ is zero for a strictly plane crack ($R_l = 1$).

This concept is similar to the one of closure pressure used in fictitious crack models. But, here, during the crack growth process, the observed phenomena could not be represented by a unique cohesive crack but rather by a succession of cohesive cracks with tip singularities (according to the classification and the terminology used by Elices and Planas [16]). Generally, sophisticated relations are always assumed according to the crack widening. These relations rely on the softening branch that is observed in direct tension tests. Here, it must be emphasized that, even in direct tension tests, there is always propagation of a crack across a section.

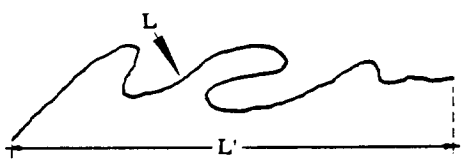

FIGURE 7. Linear roughness R_l = L/L'.

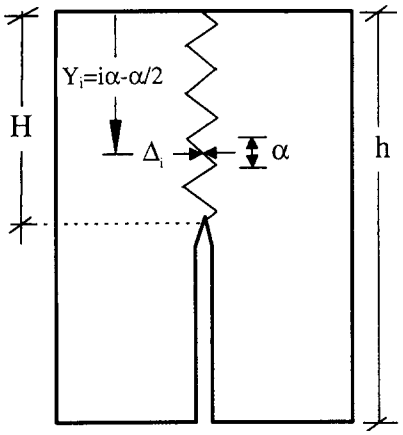

FIGURE 8. Crack profile roughness model.

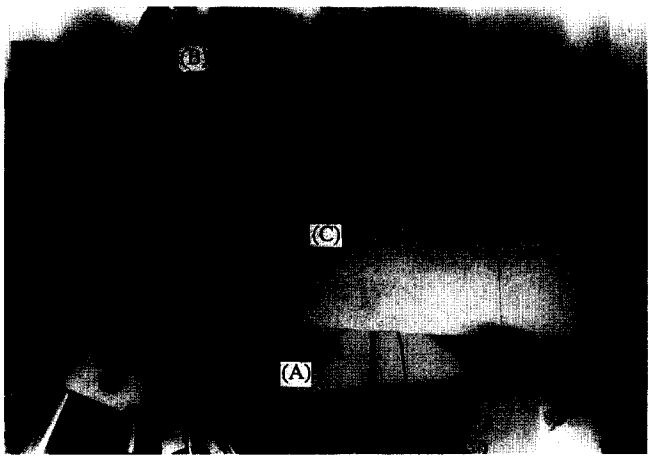

FIGURE 9. Photograph of the specimen during the test. LVDT (A) measures the crack opening (Δ) under the notch, LVDT (B) measures the deflection (δ), and five gauges (C) are used to measure the crack-opening distribution (Δ_i) along the ligament of the specimen.

Thus, softening is not representative of an intrinsic material behavior, because it results from a structure mechanism. This can be corroborated by all the attempts of concrete fracture modeling with different shapes of softening branch [17]. So the constant force Φ may be regarded as a rough but realistic approximation.

For the ith step, when the mean crack opening increases from zero to Δ_i, the RCW force Φ induces a dissipation of energy $E_{\Phi i}$ which depends on the opening of the crack:

$$\Delta_i \leq \Delta_c, \quad E_{\Phi i} = K(R_l - 1)\Delta_i \tag{6}$$

and

$$\Delta_i \geq \Delta_c, \quad E_{\Phi i} = K(R_l - 1)\Delta_c \tag{7}$$

Crack Opening

CRACK OPENING ALONG THE LIGAMENT. Tests were carried out on specimens to determine the distribution of the crack openings along the ligament. Five strain gauges used as displacement transducers (the procedure has been described by Turatsinze [8]) were distributed along the ligament. A linear variable differential transformer (LVDT) was placed at 10 mm under the notch. Each one was located by its position Y_i and measured the displacement Δ_i (noted Δ for the LVDT, which defines the crack-opening level). Such a specimen is represented by the photograph in Figure 9. The measured parameters and the location of the used gauges (G1 to G5) are illustrated in Figure 10. Figure 11 gives an example of recorded curves resulting from the application of such a test.

The crack-opening distributions that occurred beyond the peak of the load-deflection curve are drawn in Figure 12. One can notice that Δ_i is a linear function of the position of measure Y_i. This is in accordance with the kinematic block theory in fracture mechanics of mortar and concrete. In the remainder of this paper, we will always be dealing with specimens loaded up to obtain linear crack-opening distributions.

$$\Delta_i(\Delta) = CY_i \tag{8}$$

where C depends on the level of the crack opening Δ measured under the notch. It does not depend on the ligament length H.

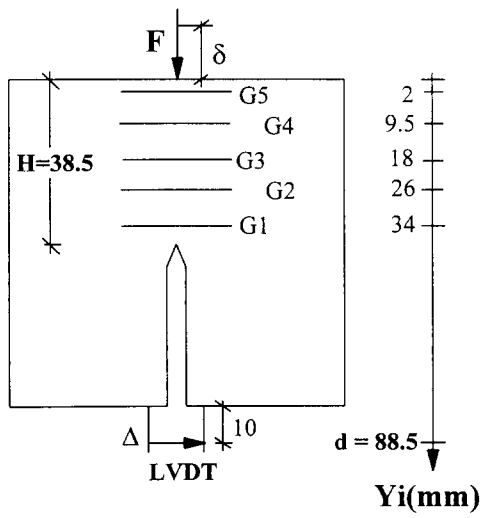

FIGURE 10. Location of the different points of measurement.

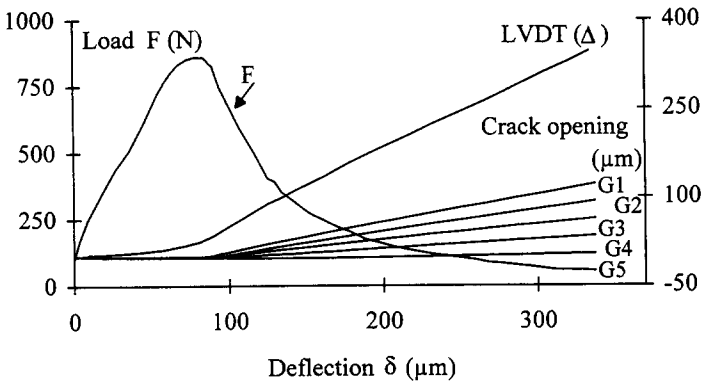

FIGURE 11. Load (F) and crack opening (Δ_i) according to the deflection (δ) of the point of load application.

According to eq 8, the crack opening at the notch tip Δ_0 is

$$\Delta_0(\Delta) = CH \tag{9}$$

with

$$C = \frac{\Delta}{d} \tag{10}$$

where Δ is the displacement measured by the LVDT whose distance from the upper fiber of the specimen is marked d (Figure 10).

RELATIONSHIP BETWEEN THE FRACTURE ENERGY AND THE SPECIMEN LIGAMENT LENGTH. Two cases have to be considered:

1. As long as there is no effective separation of the two crack surfaces ($\Delta_i < \Delta_c$), eq 6 can be written like

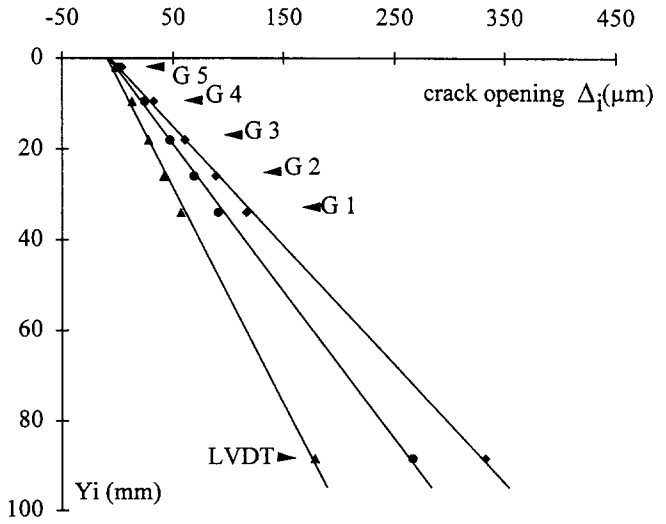

FIGURE 12. Crack-opening distribution (Δ_i) according to the location (Y_i) of the point of measurement.

$$E_\Phi(H,\Delta) = K(R_l - 1)C\Sigma Y_i \tag{11}$$

According to relation 3

$$E_\Phi(H,\Delta) = K(R_l - 1)C\left(\alpha + 2\alpha + 3\alpha + \ldots + n\alpha - \frac{n\alpha}{2}\right)$$
$$= K(R_l - 1)C\left(\frac{n\alpha(n+1)}{2} - \frac{n\alpha}{2}\right)$$

From relation 4 we can write

$$E_\Phi(H,\Delta) = \frac{K(R_l - 1)}{\alpha} C\frac{H^2}{2} \tag{12}$$

Considering a specimen with a ligament length H, the energy dissipated by RCW is:

$$E_\Phi(H,\Delta) = \beta CH^2 \tag{13}$$

where

$$\beta = \frac{K(R_l - 1)}{2\alpha} \tag{14}$$

For a specimen whose width is equal to the unit, the total energy per unit of crack sufrace $\gamma_{A(H,\Delta)}$ is

$$\gamma_A(H,\Delta) = \gamma_C + \frac{E_\Phi(H,\Delta)}{H} = \gamma_C + \beta CH \tag{15}$$

2. This linear relation is no longer valid if the crack opening exceeds the critical value Δ_c. For the part of the crack whose opening reaches or exceeds the critical value Δ_c, the RCW vanishes and an additional increasing of the crack opening does not induce a dissipation of energy. This case is illustrated in Figure 13. In these conditions, we must

Advn Cem Bas Mat
1996;4:77–92

consider that RCW remains active solely on a part of the ligament X on which relations 13 and 15 are still valid. For the whole ligament, the energy dissipated is

$$E_\Phi(H,\Delta) = \beta C X^2 + K(R_l - 1)\frac{H - X}{\alpha}\Delta_c \qquad (16)$$

So, the fracture energy per unit of crack surface may be written like:

$$\gamma_A(H,\Delta) = \gamma_C + \frac{E_\Phi(H,\Delta)}{H}$$

$$= \gamma_C + \frac{\beta C X^2}{H} + 2\beta\frac{(H - X)}{H}\Delta_C$$

writing

$$\omega = 2\beta\Delta_c \qquad (17)$$

γ_A can be expressed by the hyperbolic relation:

$$\gamma_A(H,\Delta) = \gamma_C + (\beta C X - \omega)\frac{X}{H} + \omega \qquad (18)$$

For a given composition, it is reasonable to consider the parameters β, Δ_c (and therefore ω) as constant.

Theoretical Variation of the Fracture Energy per Unit of Crack Surface

According to eqs 15 and 18, γ_A depends on both the initial ligament length H and the crack-opening level. The function C depends on the crack opening level whereas the parameters β and Δ_c can only be deduced from the experimental results.

Let us accept these parameters as given. According to the crack-opening level Δ, the length X concerned by the RCW can be calculated

$$X = \Delta_c\frac{d}{\Delta} \qquad (19)$$

Two cases may occur:

1. $H < X$. The critical crack opening Δ_c is not reached anywhere along the ligament. Then, the fracture energy per unit of crack surface γ_A is calculated according to relation 15 and γ_A is a linear function of H.
2. $H \geq X$. The crack opening reaches or exceeds the critical value Δ_c on a part of the crack path. Then γ_A is calculated according to relation 18. It has to be pointed out that when the crack opening Δ increases, the part X of the ligament concerned by the RCW decreases, and at the end tends to zero. In these conditions, γ_A tends to the constant value $\gamma_c + \omega$ and the size dependence on γ_A tends to vanish.

Consequently, for a given crack-opening level Δ, the variation of the fracture energy per unit of crack surface γ_A versus the initial ligament length H results in a linear diagram for $H < X$ followed by an hyperbolic branch for $H \geq X$ as it is illustrated in Figure 14.

The slope of the straight line is equal to βC. According to relation 10, C is related to Δ and the constant β can be deduced. C and the slope βC increase with Δ. On the other hand, the intersection with the γ_A axis determines the term γ_C.

It has to be noticed that the dependence of γ_A on Δ can be related with the influence of P-δ tail cutting [18] on the measured fracture energy by means of the RILEM TC-50 procedure. Indeed, using this procedure, a decision to stop the tests somewhere in the descending branch of the load-deflection diagram has to be taken. Consequently, a part of the fracture energy is neglected. However the comparison between the impact of P-δ tail cutting [18] and the model we propose here must be restricted. There are two salient differences: first, we introduce an effect of RCW that results in the energy per unit of crack surface γ_Φ. Second, the RCW takes place as soon as the crack propagates, and it acts until the crack opening reaches the critical value Δ_c. Consequently, the influence of the RCW on the fracture energy cannot be limited to the energy neglected by P-δ tail cutting.

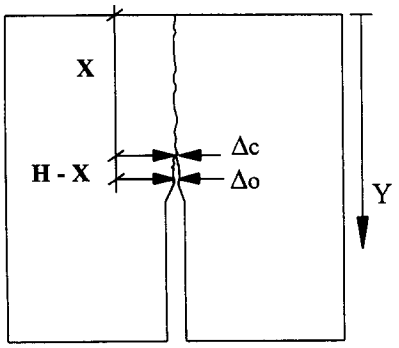

FIGURE 13. Critical crack opening (Δ_C) definition and effective separation. $Y < X$; $\Delta < \Delta_C$. There is no effective separation. $X \leq Y \leq H$; $\Delta \geq \Delta_C$. There is effective separation.

Experimental Results

Experimental Program

To test the validity of our model, it was necessary to compile test data about fracture energy determined by

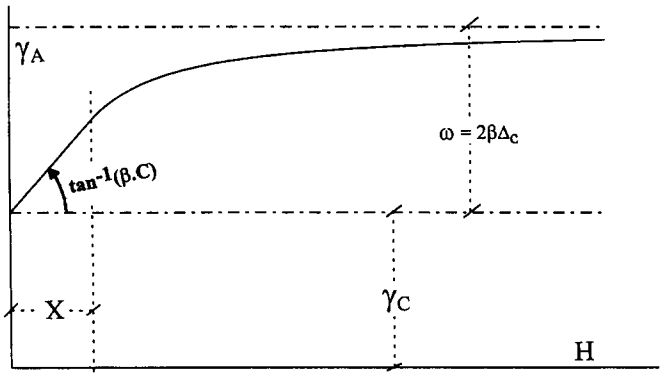

FIGURE 14. Theoretical variation of the fracture energy per unit of crack surface γ_A.

integration of the load-deflection relationship [13] for various ligament lengths and various roughness conditions. Here we present the results of tests performed for this purpose. Our mechanical device allowed us to vary the ligament length from 20 mm to 70 mm for beams 80 mm in depth. Concerning roughness conditions, it is known that the path of the crack in mortar and concrete is generally located at the transition zone [19]. So, the profile of fracture surfaces depends on the size of the aggregate, and it was assumed that the sinuosity of the crack path and the critical crack opening Δ_c increase with the maximum aggregate size d_{max}.

The ideal way to point out the influence of the maximum aggregate size d_{max}, and that of the roughness of the crack on the energy dissipated by RCW, would be to test specimens with the same matrix but different d_{max}. In such conditions, it would be sensible to consider γ_C as constant, and it would be possible to impute the observed variation on the energy per unit of crack surface solely to the variation of the maximum aggregate size. Unfortunately, even if we leave out the variation of the maniability of the mix, the microstructure of the matrix is changed when the aggregate size is changed. Indeed, the water to cement (w/c) ratio of the transition zone is different from that of the matrix [20]. If the aggregate size is varied, the developed matrix-aggregate interface is changed as is the w/c ratio of the matrix. Thus, concerning the influence of the aggregate size, we will merely observe the variation of the term γ_Φ, which essentially depends on the crack sinuosity. It is expected to increase with the maximum aggregate size.

Three mixes (I, II, and III) have been studied. Crushed marble has been used as aggregate. For the reason discussed earlier, the mix proportions are chosen for the maniability without any concern to maintain a constant matrix. Their main characteristics are given in Table 2.

For each test, three or four samples were available. During the test, the load F, the deflection δ, and the crack-opening level Δ at 10 mm under the notch were recorded. Some values of Δ were fixed, and for each one the corresponding deflection δ was determined. The dissipated energy E_A was determined according to these values of δ. Figure 15 illustrates the evolution of the measured parameters and the way of determination of the dissipated energy E_A.

First, we calculated a rough energy E_{Ameas}, ($E_{Ameas} = W + mg\delta/2$). Next, a value of fracture energy per unit of crack surface γ_{Ameas} was deduced by dividing the dissipated energy E_{Ameas} by the area S of the initial ligament.

The energies dissipated by crushing γ_P and by friction γ_F at the supports were subtracted from γ_{Ameas} to obtain the fracture energy per unit of crack surface γ_A:

$$\gamma_A = \gamma_{Ameas} - \gamma_P - \gamma_F \tag{20}$$

The energy dissipated by crushing γ_P [21] was evaluated according to the conclusions of Ramoda [22] who determined this energy for the same specimen geometry, particularly the same beam span, that we used in our tests. According to this author, we can write the following relation

$$\frac{\gamma_P}{\gamma_{Ameas}} = -0.26\frac{a}{h} + 0.21 \tag{21}$$

TABLE 2. Main characteristics of the studied mixes

Components	Mix I	Mix II	Mix III
Water (l/m^3)	352	296	204
Cement CPA HP (kg/m^3)	664	557	385
Aggregate (kg/m^3)	1169	1455	1629
d_{max} (mm)	0.4	3.15	16
Compressive strength σ_c (MPa)	45.7	47.5	49.9
Young modulus (GPa)	24.1	27.1	36.7

Advn Cem Bas Mat
1996;4:77–92

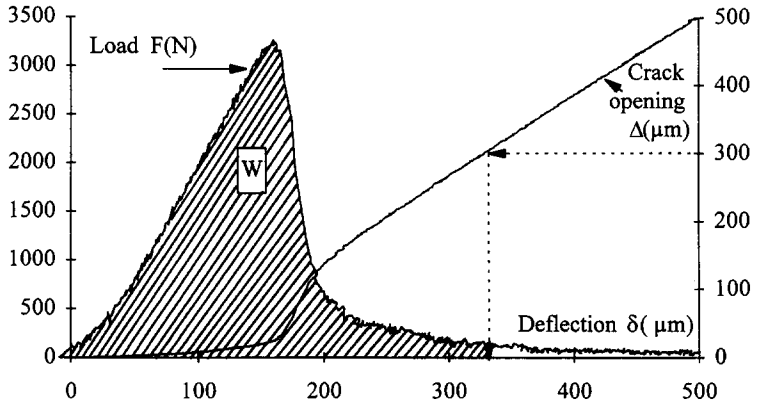

FIGURE 15. Determination of the energy dissipated during a test according to the crack opening (Δ). Mix III, ligament length H = 70 mm, Δ = 300 μm, $E_{Ameas} = W + mg\delta/2$, where m is the weight of the sample and g the acceleration due to gravity.

where a is the depth of the notch of the specimen, and h the specimen depth. In our tests, h is constant and is equal to 80 mm.

The energy γ_F dissipated by friction at the supports was determined according to Guinea et al. [23] by considering a simplified rigid-body kinematics. For our specimen geometries, the measured energy per unit of crack surface γ_{Ameas} and the actual energy per unit crack surface γ_A are linked by the relation:

$$\frac{(\gamma_{Ameas} - \gamma_P) - \gamma_A}{\gamma_A} = \frac{2\mu\frac{h}{B}}{1 - 2\mu\frac{h}{B}}$$

where μ is the friction coefficient at the supports, with μ = 0.3, h = 80 mm, and B = 320 mm:

$$\frac{\gamma_{Ameas} - \gamma_P - \gamma_A}{\gamma_A} = \frac{\gamma_F}{\gamma_A} = 0.18 \qquad (22)$$

So, taking into account eqs 21 and 22, eq 20 may be written like

$$\gamma_A = \left(0.67 + 0.22\frac{a}{h}\right)\gamma_{Ameas} \qquad (23)$$

Three crack-opening levels have been considered: Δ = 100, 200, and 300 μm for mixes I and II, 200, 300, and 400 μm for mix III. For mixes I and II, the experimental load-crack opening diagrams showed that the samples generally broke for a crack opening Δ between 300 and 400 μm. Concerning mix III, a crack opening inferior to 200 μm did not yet ensure a linear distribution of the crack opening along the specimen ligament. The energy per unit of crack surface γ_A was calculated for each mix according to these crack opening levels. Results are given in Table 3.

Determination of the Parameters γ_c, β, and Δ_c

For each mix, the parameters have been determined from the results corresponding to the lower crack opening Δ (100 μm for mixes I and II, 200 μm for mix III) as reported earlier. We describe in detail, in the Appendix, the way we determined the parameters γ_c, β, and Δ_c.

As the factor C is linked to Δ by means of relation 10, the parameter β can be deduced from the slope βC of the linear branch whose intersection with the γ_A axis determines the γ_C value. In the procedure, the last square method is applied to fit the hyperbolic branch and to determine the parameters X and ω. Then, the critical crack opening Δ_c is deduced from relation 17.

Moreover, the linear branch and the hyperbolic one must be continuously jointed. Taking into account eqs 17 and 19, this implies that the following relation has to be satisfied:

$$X = \frac{\omega d}{2\beta\Delta} \qquad (24)$$

Table 4 gives the values of γ_C, β, and Δ_c determined by this procedure. The corresponding curves are drawn in Figures 16a, 17a and 18a. All X values are reported in Table 5.

Application of the Model to Higher Crack-Opening Levels

The proposed model must be able to predict the variation of the energy per unit of crack surface γ_A versus the initial crack length H for any higher Δ value. For a given crack-opening level Δ, the factor C is calculated from

TABLE 3. Experimental fracture energy per unit of crack surface γ_A (N/m)

	Mix I			Mix II			Mix III		
	Δ (μm)			Δ (μm)			Δ (μm)		
H (mm)	100	200	300	100	200	300	200	300	400
20	15.5	21.4		25.4	32.0	35.0	29.8	34.2	
20	17.4	22.4	24.9	24.6	29.8	30.3	37.4	42.6	50.3
20	16.1	20.4	22.7	23.0	28.9	30.2	31.2	35.9	44.0
20	11.8	16.1	18.5				39.5	46.7	56.3
30	19.9	22.1	23.4	28.5	33.9		43.3	48.6	57.9
30	18.3	21.0	22.6	25.7	29.4		39.8	44.6	53.9
30	19.8	21.9	23.9	28.8	34.0	35.6	43.4	47.4	54.9
30	18.3	20.7	22.0				46.5	51.7	60.8
40	13.9	15.7	15.8	25.1	30.2	32.5	60.5	66.5	73.3
40	14.3	16.7	17.2	25.5	30.3	31.8	47.2	51.4	57.2
40	12.0			27.2	37.2	41.2	51.1	55.7	61.2
40							42.8	46.7	52.0
50	22.8	23.7	23.7	33.2	35.4	36.0	55.6	58.9	60.7
50	22.6	24.3	24.5	30.2	32.8	33.4	62.7	67.1	69.7
50	27.0	28.2	28.4	40.2	43.1	43.8	60.8	66.1	68.9
50	22.6	24.1	24.4				56.3	60.0	62.2
60	22.8	25.7	27.0	35.1	36.1		52.2	54.7	55.7
60	24.9	27.6	28.5	29.6	32.6	33.2	56.0	57.8	58.6
60	18.1	20.2	21.5	32.0	34.1	33.6	52.0	54.5	55.9
60	22.3	25.1	26.2						
70				33.8	36.8	38.1	66.2	69.9	71.7
70				37.1	40.7	42.3	58.2	61.5	62.9
70				30.4	34.2	35.8	61.5	65.1	66.7
70				41.8	45.3	47.1	55.9	58.6	60.2

relation 10 and the length X can be deduced from relation 19 according to the critical value Δ_c of the mix yet determined.

Then, applying relations 15 and 18, new curves of variation of the energy per unit of crack surface γ_A versus the initial ligament length H can be drawn. This is illustrated by the dotted curves in Figures 16b and 16c for mix I and, respectively, $\Delta = 200$ μm, $\Delta = 300$ μm; in Figures 17b and 17c for mix II and, respectively, $\Delta = 200$ μm, $\Delta = 300$ μm; and in Figures 18b and 18c for mix III and, respectively, $\Delta = 300$ μm, $\Delta = 400$ μm.

The experimental results have been reported in these figures with, in each case, the correlation coefficient between the experiment average values and the ones from the model. In addition, Figure 19 shows the correlation between all the experimental values of γ_A with the predicted ones by the model. We obtain a linear correlation coefficient of 0.98. Moreover, the linear regression gives rise to a straight line very close to the dotted bisecting line in the diagram.

TABLE 4. Parameters of the model (parameters determined for the minor crack opening level)

Measures	Mix I	Mix II	Mix III
γ_c (Nm^{-1})	6	15	20
β (MPa)	0.41	0.38	0.36
Δ_c (μm)	28	36	70
ω (Nm^{-1})	20.8	26.4	50.1

Discussion

Some comments have to be made with regard to the initial hypotheses.

RCW can be considered as a material property. Because we still observe size-dependent values for the fracture energy per unit of crack surface according to various ligament length (all the dimensions being kept constant), this property, in turn, leads to a structural effect. In that sense, our results point towards an R-curve behavior.

The specific fracture energy with Griffith's sense γ_c is an average value including the energy necessary for the crack propagation in the matrix and at the interfaces. If we consider the specific fracture energy as intrinsic to the material, one can notice that with a single specimen length, this energy is not directly accessible by using the RILEM TC-50 procedure. It is included in the fracture energy per unit of crack surface in which the part due to the RCW depends on the kinematic block separation. γ_c must depend on the proportion and the nature of the mix components. So, the observed increase of γ_c with the maximum aggregate size (see Table 4) cannot be generalized.

When the whole ligament is still subjected to the RCW ($X \geq H$), Figures 16b, 17b, and 18a show that for the same crack-opening level $\Delta = 200$ μm the slopes βC of the three diagrams are almost identical for the three

Advn Cem Bas Mat
1996;4:77–92

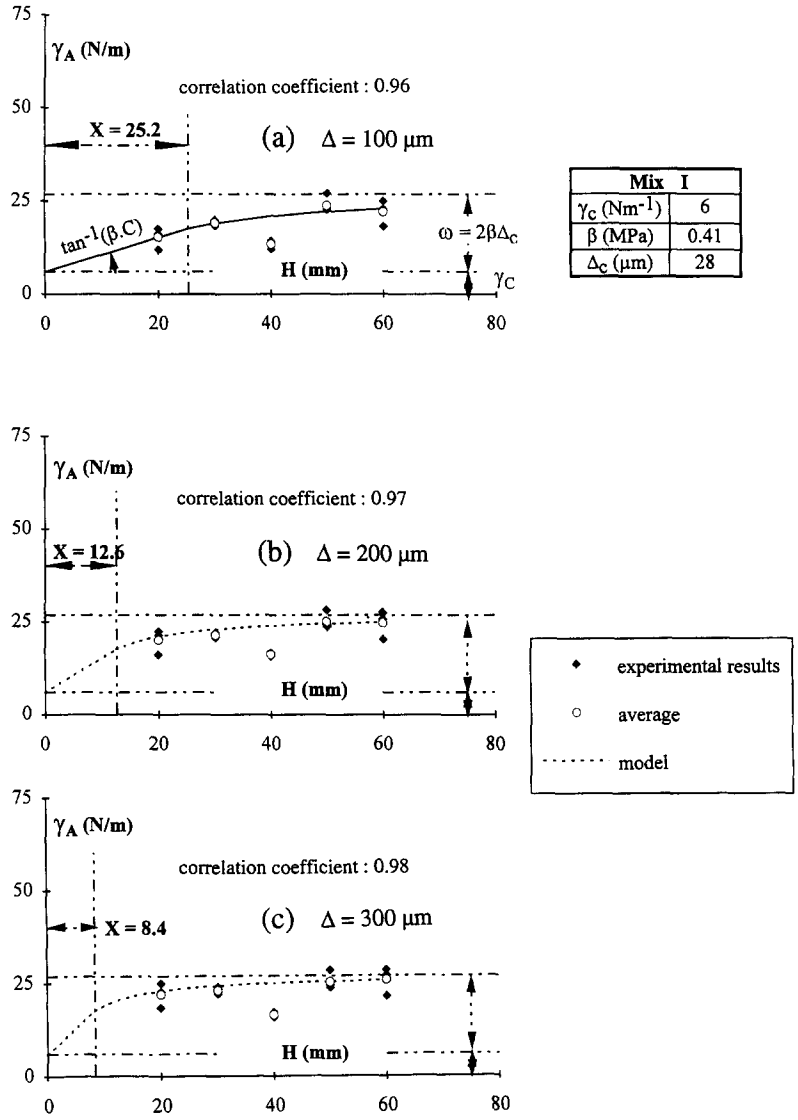

Mix I	
γ_c (Nm^{-1})	6
β (MPa)	0.41
Δ_c (μm)	28

FIGURE 16. In mix I, variation of the fracture energy per unit of crack surface γ_A.

mixes. Because the factor C is constant in these cases, β values must be very close to each other as it can be seen in Table 4. This indicates that the variation of the studied mix components slightly influences the parameters β. On the other hand, Table 4 shows that the critical crack opening Δ_c logically increases with the maximum aggregate size. So, according to relation 17, the RCW must be more significant for the mix with the greater aggregate size. It must vanish more quickly for a mix with a small aggregate size, because, in that case, the critical crack opening Δ_c is lower. All these observations are consistent with the experimental data. Particularly, one can notice that the asymptotic value (γ_c + ω) is reached more quickly for the mix with the smaller aggregate size (mix I).

Finally, the critical crack openings Δ_c determined by means of the proposed model are close to critical widths measured through the independent experiments [24]. This gives support to the physical meaning of the RCW model.

Conclusions

Direct and microscopical observations by means of the replica technique in conjunction with scanning electron microscopy were carried out on notched beams in three-point bending tests. They give a new insight into the tip of the crack and the fracture process zone.

Indeed, a sinuous and continuous single crack path was observed on the lateral surface of the specimens. Inside the material, the continuous crack path was always followed by discontinuous microcracks. However, these microcracks were not distributed at random. They anticipated the future continuous crack path.

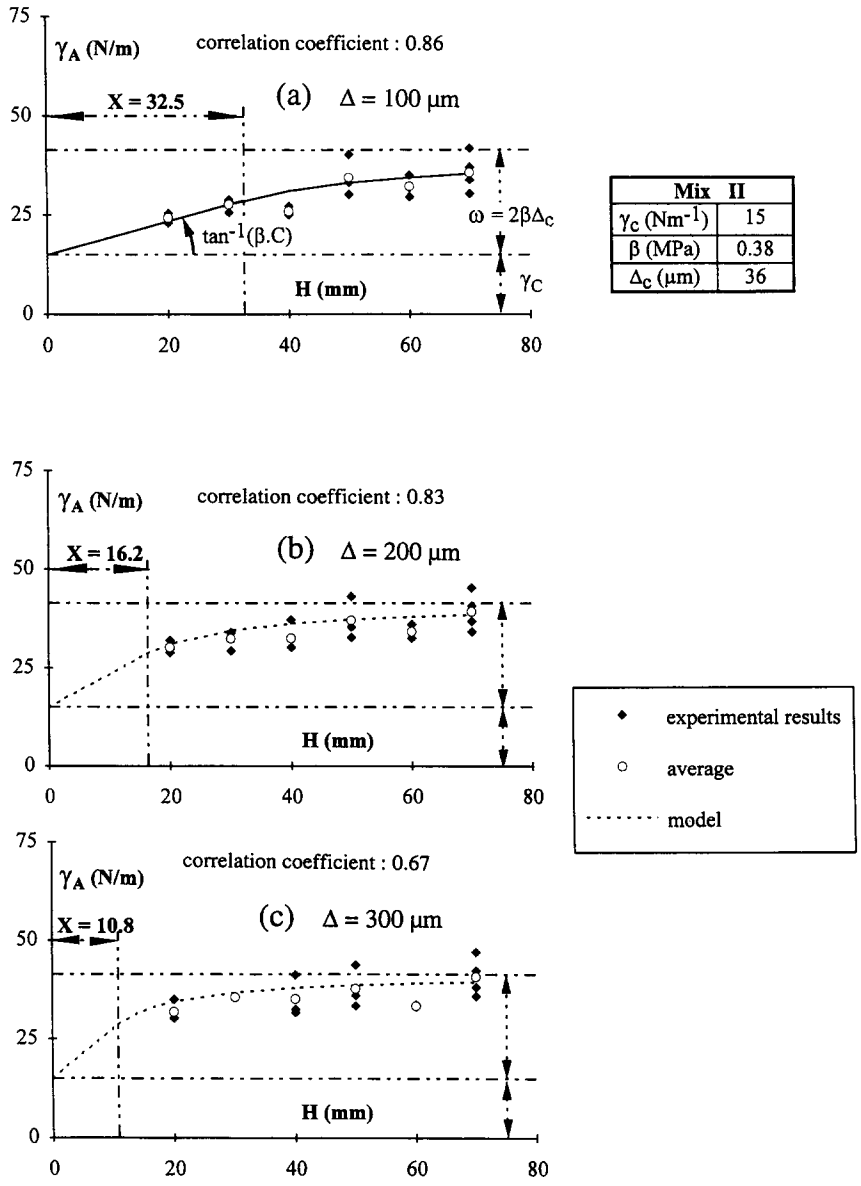

Mix II	
γ_c (Nm^{-1})	15
β (MPa)	0.38
Δ_c (μm)	36

FIGURE 17. In mix II, variation of the fracture energy per unit of crack surface γ_A.

So, except for a few crack branches, we can consider that the complete fracture of a specimen induces a single rough crack surface. Therefore, in the cases where the mechanical test gives rise to a localized strain gradient, the main cause of the size dependence affecting the fracture energy per unit of crack surface may not be the formation of a cloud of microcracks around the tip of the continuous crack path and has to be investigated elsewhere. It may be found through a phenomenon of RCW. This phenomenon is essentially due to the roughness of the crack surfaces that has been presumed to be dependent on the maximum aggregate size.

During the crack opening, RCW forces are induced and an energy is dissipated. We assumed that this energy is added to the one necessary for the crack propagation in Griffith's sense. So, we have proposed a simple model of fracture energy dissipation including the part due to the RCW effect. Then, the fracture energy per unit of crack surface γ_A is the sum of two terms: the specific fracture energy in Griffith's sense (γ_C) and the term due to the RCW phenomenon (γ_Φ).

We tried to validate this theoretical approach. For this purpose, the fracture energy was measured from three-point bending tests by means of the area under the load-deflection curve. The aggregate size and the ligament length were varied. Finally, it was possible to fit the parameters of our model to the observed variation of the fracture energy per unit of crack surface.

So, even if it may not be asserted that it is the unique

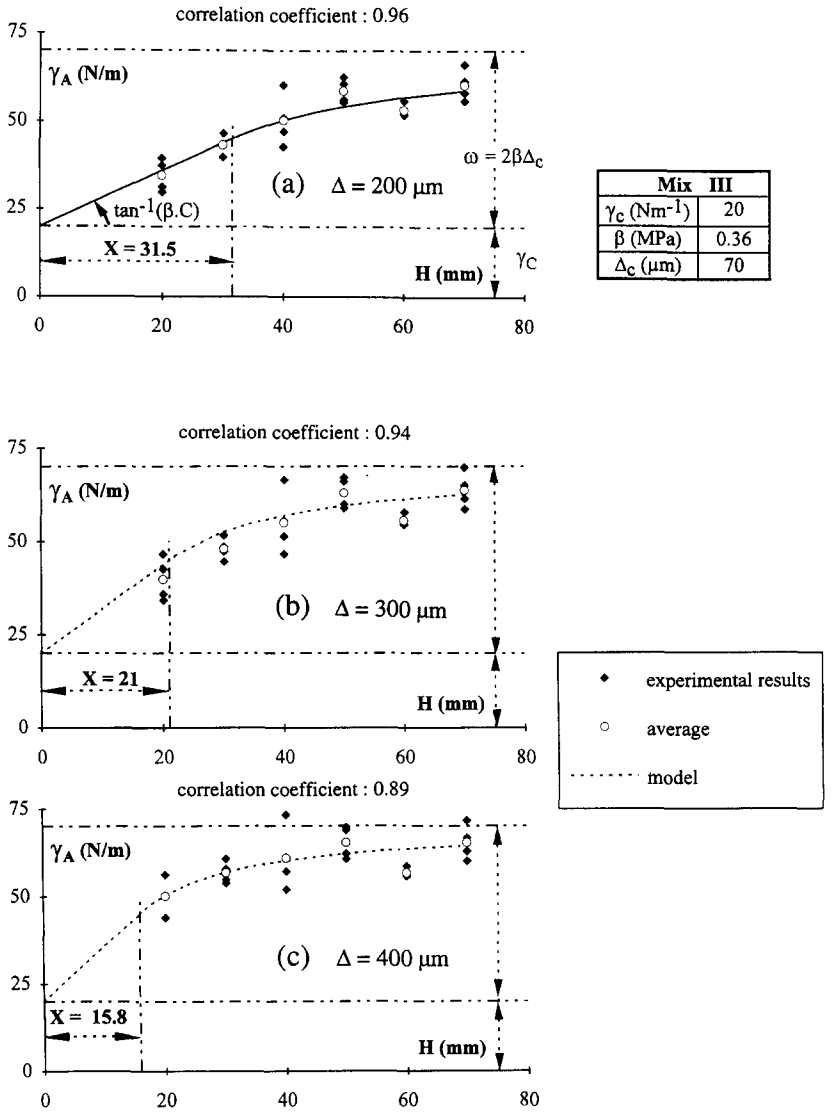

Mix	III
γ_c (Nm^{-1})	20
β (MPa)	0.36
Δ_c (μm)	70

FIGURE 18. In mix III, variation of the fracture energy per unit of crack surface γ_A.

phenomenon to be taken into account, it can be concluded that RCW seems to be a main source of size dependence in mode I crack propagation for mortar and concrete. However, the proposed model has to be improved. Particularly, the RCW forces have been considered as constant during the crack opening. This is a rough approximation. We also subjectively considered the RCW and the critical crack opening as linked. We estimated that they increase with the roughness that increases with the maximum aggregate size d_{max}. This argument is not fully justified. Indeed, one can presume a prominent interlocking effect with a minor roughness effect. For these reasons, it is fundamental to develop work about the measurements of the roughness and a more realistic evaluation of these RCW forces. We have already begun to make roughness measurements [8]. The measured values are magnification dependent, and the roughness appears to have a semifractal dimension. This result, obtained by means of the method of Mandelbrot-Richardson, is illustrated in Figure 20. Similar results are proposed by other authors [25,26].

TABLE 5. Length X still subjected to RCW according to the crack opening level Δ (μm)

	X (mm)		
Δ (μm)	Mix I	Mix II	Mix III
100	**25.2**	**32.5**	
200	12.6	16.2	**31.5**
300	8.4	10.8	21.0
400			15.8

Notation

RCW restrained crack widening

a depth of the notch

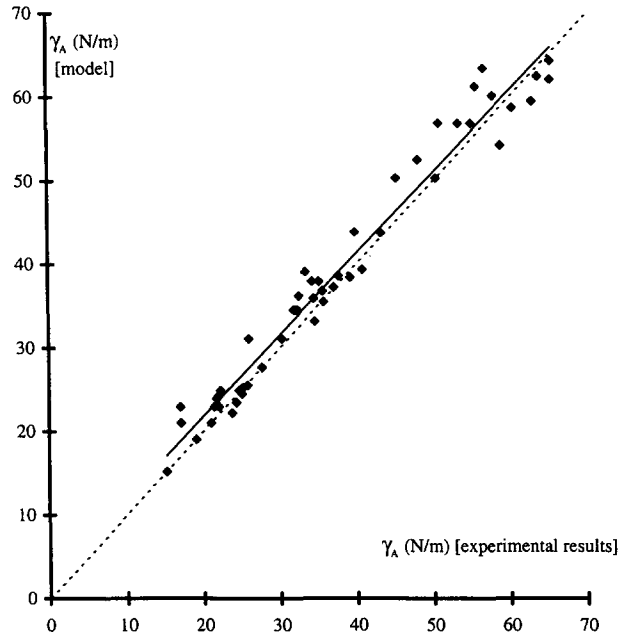

FIGURE 19. Correlation between the experimental values of γ_A and the predicted ones by the model.

B	beam span
C	opening coefficient
d	distance between the upper fiber of the specimen and the LVDT axis used for Δ measurements
d_{max}	maximum aggregate size
E_A	apparent fracture energy
E_{Ameas}	rough energy dissipated during a test
E_C	energy for the initiation and the propagation of the crack
E_Φ	energy dissipated by RCW during the increase of the crack opening
$E_{\Phi i}$	energy dissipated by RCW for a step i of the crack profile
F	applied load
g	acceleration due to gravity
H	specimen ligament length
h	specimen depth
K	coefficient characterizing the crack profiles
m	weight of a sample
R_l	linear roughness
S	projected crack surface
W	area under the load-deflection curve
X	part of the ligament on which RCW remains active
α	step length of the periodic crack profile
β	resultant force Φ divided by half step length α
Δ	crack opening measured under the notch
δ	displacement of the load application point
Δ_0	crack opening at the notch tip
Δ_C	critical crack opening for an effective separation of the two crack surfaces
Δ_i	main crack opening for a step i of the crack profile
Φ	resultant force due to RCW acting on a step of the crack profile
γ_A	fracture energy per unit of crack surface
γ_C	specific fracture energy in Griffith's sense
γ_Φ	energy due to RCW per unit of crack surface
γ_F	energy per unit of crack surface dissipated by friction at the supports
γ_{meas}	measured fracture energy per unit of crack surface including crushing and friction effects at the supports
γ_P	energy per unit of crack surface dissipated by crushing
μ	friction coefficient at the supports
ω	energy per unit of crack surface dissipated by RCW when the crack opening increases from zero to the critical value Δ_C

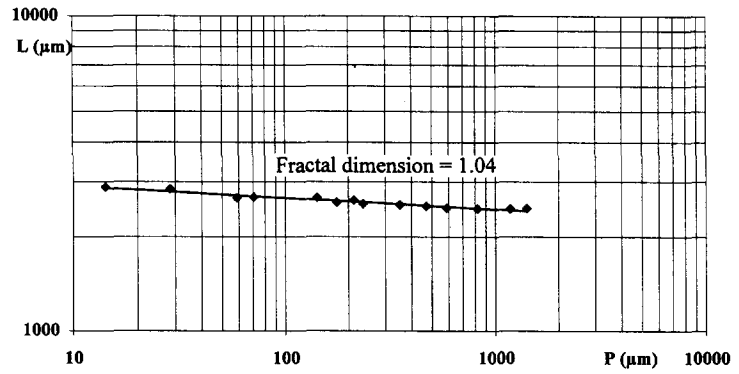

FIGURE 20. Example of measurement of a crack length L versus the size of the measurement step P by means of the Mandelbrot-Richardson method. Log –Log plot; mix II – H = 40 mm.

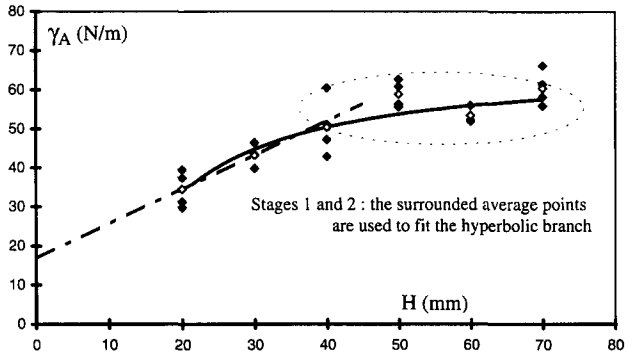

FIGURE A1. Mix III – $\Delta = 200$ μm; $\gamma_C = 16.9$ N/m; $\omega = 50$ N/m; X = 21.3 mm.

Appendix: Determination of the Model Parameters

Parameters of γ_C, β, and Δ_c are determined for each mix, according to the lower Δ opening.

In a first stage, the two first average experimental points are used to propose a linear branch. First, values for γ_C and the slope βC are derived; C being fixed, β is deduced.

In a second stage, the values of γ_C, β, and C are used in relation 18 to fit an hyperbolic branch to the remaining average experimental points: then parameters X and ω are solved by means of least square method. For the abscissa $H = X$, the linear branch and the hyperbolic branch must be continuously connected.

In a third stage, if a difference between the slopes of the two branches at their intersection ($H = X$) is observed, all the determined parameters are not satisfying and the procedure has to be continued. The linear branch is modified. Then, there is a return to stage two. These readjustments are repeated until satisfying parameters are found (independently of the number of experimental points in the domain of the linear branch).

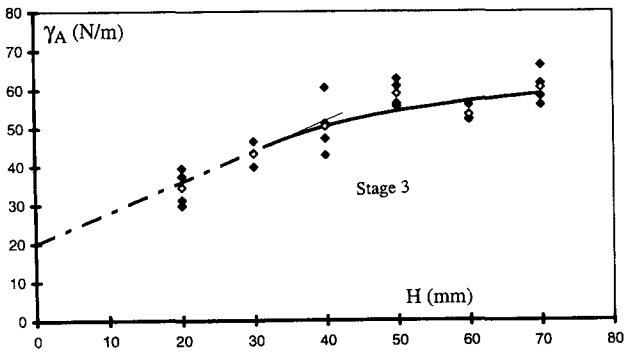

FIGURE A2. Mix III – $\Delta = 200$ μm; $\gamma_C = 20$ N/m; $\omega = 50.1$ N/m; X = 31.5 mm.

The procedure ends when the linear part and the hyperbolic one are continuously jointed. Figures A1 and A2 are given for examples. Finally, the critical crack opening Δ_C is deduced according to relation 17.

References

1. Mindess, S. In *Fracture Mechanics. Test Methods for Concrete;* Shah, S.P.; Carpinteri, A., Eds.; Chapmann & Hall: London, 1991; pp 231–255.
2. Swartz, S.E.; Go, C.-G. *Exper. Mech.* **1984,** *24,* 129–134.
3. Bascoul, A.; Kharchi, F.; Maso, J.-C. In *SEM/RILEM International Conference on Fracture of Concrete and Rock, Houston;* Shah, S.P.; Swartz, S.E. Eds.; Society of Experimental Mechanics: Bethel CT, 1987; pp 396–408.
4. Van Mier, J.G.M. *Mode I Fracture of Concrete: Discontinuous Crack Growth and Crack Interface Grain Bridging,* Report 25.5-90-7/VFA; Delft University of Technology, 1990.
5. Ollivier, J.P. *Cem. Concr. Res.* **1985,** *15,* 1055–1060.
6. Bascoul, A.; Détriché, Ch.-H.; Ollivier, J.-P.; Turatsinze, A. In *Proceedings of the International Conference on Recent Development in Fracture of Concrete and Rock;* Shah, S.P., Swartz, S.E.; Barr, B. Eds.; Elsevier Applied Science, 1989; pp 327–336.
7. Bascoul, A.; Turatsinze, A. In *Proceedings of the First International Conference on Fracture Mechanics of Concrete Structures;* Bazant, Z.P., Ed.; Elsevier, 1992; pp 503–508.
8. Turatsinze, A. Thèse de doctorat de l'Université Paul Sabatier, Toulouse, 1992.
9. Bascoul, A.; Turatsinze, A. *Mater. Struct.* **1994,** *27,* 71–78.
10. Rossi, P. *Fissurabilité du béton: du matériau à la structure. Application de la mécanique linéaire de la rupture;* Rapport de recherche LCPC N°150; 1988.
11. Karihaloo, B.L.; Nallathambi, P. In *Fracture Mechanics of Concrete. Test Methods for Concrete;* Shah, S.P.; Carpintari, A., Eds.; Chapman & Hall: London, 1991; pp 1–69.
12. Shah, S.P. *ACI Mater. J.* **1990,** May–June, 260–265.
13. Hillerborg, A. *Mater. Struct.* **1985,** *18,* 291–296.
14. Raiss, M.E.; Dougill, J.W., Newman, J.B. *Mag. Concr. Res.* **1990,** *42,* 193–202.
15. Bazant, Z.P.; Oh, B.H. *Matériaux et Constructions* **1983,** *93,* 155–177.
16. Elices, M.; Planas, J. In *Fracture Mechanics of Concrete Structures;* Elfgren, L., Ed.; Chapman & Hall: London, 1989; pp 16–66.
17. Guinea, G.V. *Mater. Struct.* **1995,** *28,* 187–194.
18. Elices, M.; Guinea, G.M.; Planas J. *Mater. Struct.* **1992,** *25,* 327–334.
19. Maso, J.C. *La liaison pâte-granulat;* Le béton hydraulique, Presses de l'ENPC, 1982; pp 247–259.
20. Barrioulet, M.; Legrand, C. *Mater. Struct.* **1977,** *10,* 365–373.
21. Planas, J.; Elices, M.; Guinea, G.M. *Mater. Struct.* **1992,** *25,* 305–312.
22. Ramoda, S. Thèse de doctorat de l'INSA, Toulouse, 1987.
23. Guinea, G.M.; Planas, J.; Elices, M. *Mater. Struct.* **1992,** *25,* 212–218.
24. Gopalaratnam, V.S.; Shah, S.P. *ACI. J.* **1985,** *82,* 310–323.
25. Lange, D.A.; Jennings, H.M.; Shah, S.P. *J. Amer. Ceram. Soc.* **1993,** *76,* 589—597.
26. Hammad, A.M.; Issa, M.A. *Adv. Cem. Based Mater.* **1994,** *1,* 169–177.